

Unveiling spatial and temporal heterogeneity of a tropical forest canopy using high-resolution NIRv, FCVI, and NIRvrad from UAS observations

Trina Merrick^{1,2}, Stephanie Pau², Matteo Detto^{3,4}, Eben N. Broadbent⁵, Stephanie A. Bohlman^{3,6}, Christopher J. -Still⁷, Angelica M. Almeyda Zambrano⁸

¹Naval Research Laboratory, Remote Sensing Division, 4555 Overlook Ave. SW, Washington, DC, 20375, USA

²Department of Geography, Florida State University, 113 Collegiate Loop, Tallahassee, Florida 32306, USA

³Smithsonian Tropical Research Institute, Apartado 0843-03092, Balboa, Ancon, Panama

⁴Department of Ecology and Evolutionary Biology, Princeton University, Princeton, New Jersey 08544 USA

⁵Spatial Ecology and Conservation Lab, School of Forest, Fisheries and Geomatics Sciences, University of Florida, Gainesville, FL, 32608 USA

⁶School of Forest, Fisheries and Geomatics Sciences, University of Florida, Gainesville, FL, 32608 USA

⁷Department of Forest Ecosystems and Society, Oregon State University, Corvallis, Oregon 97331 USA

⁸Spatial Ecology and Conservation Lab, Center for Latin American Studies, University of Florida, Gainesville, Florida 32608 USA

*² Primary author former affiliation

Correspondence to: Trina Merrick (trina.merrick@nrl.navy.mil)

Abstract. Recently, remotely-sensed measurements of the near-infrared reflectance (NIRv) of vegetation, the fluorescence correction vegetation index (FCVI), and radiance (NIRvrad) of vegetation, have emerged as indicators of vegetation structure and function with potential to enhance or improve upon commonly used indicators, such as the normalized difference vegetation index (NDVI) and the enhanced vegetation index (EVI). The applicability of these remotely sensed indices to tropical forests, key ecosystems for global carbon cycling and biodiversity, have been limited. In particular, fine-scale spatial and temporal heterogeneity of structure and physiology may contribute to variation in these indices and the properties that are presumed to be tracked by them, such as gross primary productivity (GPP) and absorbed photosynthetically active radiation (APAR). In this study, fine-scale (approx. 15cm and greater) tropical forest heterogeneity represented by NIRv, FCVI, and NIRvrad, and by lidar-derived height is investigated and compared to NIRv and EVI using unoccupied aerial system (UAS)-based hyperspectral and lidar sensors. By exploiting near-infrared signals, NIRv, FCVI, and NIRvrad emerging vegetation indicators captured the greatest spatiotemporal variability, followed by the enhanced vegetation index (EVI), then the normalized difference vegetation index (NDVI). Wavelet analyses showed the dominant spatial scale of variability of all indicators was driven by tree clusters and larger-than-tree-crown size gaps rather than individual tree crowns. NIRv, FCVI, NIRvrad Emerging indices, and EVI captured variability at smaller spatial scales (~50 m) than NDVI (~90 m) and lidar-based surface model (~70 m). We show that spatial and temporal patterns of NIRv and FCVI were virtually identical for a dense green canopy, confirming predictions in earlier studies. Furthermore, we show that NIRvrad, which does not require separate irradiance measurements, correlated more strongly with GPP and PAR than did other indicators. These NIRv, FCVI, and NIRvrad emerging indicators, which are related to canopy structure and the radiation regime of vegetation canopies, are promising tools to improve understanding of tropical forest canopy structure and function.

Formatted: Font: Times New Roman, 12 pt, English (United States)

Formatted: Font: Times New Roman, 12 pt, English (United States)

43 1 Introduction

44 Important spatial and temporal heterogeneity in structurally complex and species-rich tropical forests ~~is~~ not
45 well characterized. Many factors contributing to this heterogeneity, including varying microclimate, light conditions,
46 topography, crown structure, and patterns of tree mortality and regeneration, ~~contribute to~~ can produce high variability
47 in carbon fluxes, ultimately affecting coarse-scale gross primary production (GPP) measurements in
48 forests ~~heterogeneity that underlies gross primary production (GPP)~~ (e.g., Xu et al., 2015; Guan et al., 2015; Morton
49 et al., 2014; Bohlman and Pacala, 2012; Laurance et al., 2012; Clark et al., 2008; Huete et al., 2008). Improving
50 knowledge of tropical forest dynamics at multiple scales is crucial to monitoring and predicting resilience of tropical
51 ecosystems and productivity under climate change (Liu et al., 2021; Clark et al., 2017; Laurance et al., 2012; Malhi,
52 2012; Wright, 2010; Saatchi et al., 2010; Lewis et al., 2009). Remote sensing (RS) measurements have been employed
53 to uncover vegetation patterns of structure and productivity from local to global scales, often with a focus on filling
54 gaps in knowledge regarding variation and uncertainties in GPP estimates (e.g., Jung et al., 2011; Glenn et al., 2008;
55 Huete et al., 2002; Ryu et al., 2018; Yang et al., 2017; Jiang et al., 2008; Zhao et al., 2010; Heinsch et al., 2006;
56 Running et al., 2004; Turner et al., 2003). Yet, the spatial mismatch between satellite data (e.g., 30 m to 1 km pixel
57 resolution), which provides observations across large extents at repeat intervals, and site-specific plot level data (e.g.,
58 0.1 – 1 hectare), is in part responsible for the uncertainties in GPP estimates. Yet, there is a spatial mismatch between
59 satellite data (e.g., 30 m to 1 km pixel resolution), which provides observations across large extents at repeat intervals,
60 and site-specific plot level data (e.g., 0.1 – 1 hectare), is in part responsible for the ~~that contributes to~~ uncertainties in
61 GPP estimates (Gelybó et al., 2013; Zhang et al., 2020). A way to solve this problem is to acquire ~~here is a lack of~~ high
62 spatial and temporal resolution data that can capture fine-grained heterogeneity of tropical forests (Clark et al., 2017;
63 Mitchard, 2018; Saatchi et al., 2011; Lewis et al., 2009). Unoccupied aerial systems (UAS) with hyperspectral imaging
64 sensors offer ~~present~~ an opportunity to collect tropical forest canopy data at high spatial resolution and, which could
65 address unknowns related to the high heterogeneity of tropical forests.

66 Traditional reflectance-based indices (RI) using RS data, such as the normalized difference vegetation index
67 (NDVI) and enhanced vegetation index (EVI), are known to capture structural changes that are coincident with
68 changes in GPP. RIs have provided optical methods using RS to track GPP via the light use efficiency (LUE) model
69 (J.L. Monteith, 1977; Yuan et al., 2014; B. E. Medlyn, 1998). In the most commonly used formulation of the LUE
70 model for RS, GPP is

$$GPP = APAR \times \epsilon \quad (1)$$

71
72 where APAR is the absorbed photosynthetically active radiation and (ϵ) is the efficiency with which the target
73 vegetation converts the radiation to carbon (Gamon, 2015; Yuan et al., 2014; Running et al., 2004). APAR is derived
74 from

$$APAR = PAR \times fPAR \quad (2)$$

75 where PAR is the incoming photosynthetically active radiation and fPAR is the fraction of absorbed PAR. RIs
76 commonly used in the LUE model of GPP as well as direct proxies for GPP are NDVI and EVI, because of a strong
77 relationship to fPAR (Springer et al., 2017; Morton et al., 2015; Gamon et al., 2015; Porcar-Castell et al., 2014; Glenn

78 et al., 2008; Gao et al., 2007; Huete et al., 2002; Zarco-Tejada et al., 2013). NDVI and EVI are typically used as
79 proxies on seasonal timescales. ~~W, or, when~~ used to examine changes on shorter timescales, they have been multiplied
80 by photosynthetically active radiation (PAR) to account for changes in radiation (incoming, absorbed, and scattered)
81 which better align with GPP changes (Springer et al., 2017; Yuan et al., 2014). However, RIs alone have often not
82 shown enough sensitivity to capture more fine-scale or rapid changes in vegetation, such as those in tropical forests,
83 and questions linger about the ability to track green-up with RIs in evergreen regions (Liu et al., 2021; Yang et al.,
84 2018a; Lee et al., 2013; Xu et al., 2015; Morton et al., 2014; Samanta et al., 2010; Sims et al., 2008).

85 Recently, three emerging vegetation indicators have been shown to track with GPP more closely than traditional
86 RIs. These indicators are the near-infrared reflectance of vegetation (NIRv) (Badgley et al., 2017), the fluorescence
87 correction vegetation index (FCVI) (Yang et al., 2020) and the near-infrared radiance of vegetation (NIRvrad) (Wu et
88 al., 2020). Because they exploit additional information from the NIR region of the spectrum, NIRv, FCVI, and
89 NIRvrad do not saturate in dense canopies or suffer the same level of contamination from senesced vegetation and
90 soils as traditional RIs (Baldocchi et al., 2020; Badgley et al., 2017). Additionally, these ~~emerging~~ indicators require
91 only moderate spectral resolution data and are similarly straightforward to measure and calculate as RIs, making them
92 accessible in a broad range of studies. ~~In contrast, SIF measurements require very high spectral resolution and
93 multiple instruments.~~ Therefore, NIRv, FCVI, and NIRvrad could be employed as valuable indicators of canopy
94 structure ~~and function~~ (Badgley et al., 2019; Badgley et al., 2017; Dechant et al., 2020) ~~and have practical advantages
95 over making SIF measurements.~~

96 NIRv ~~is~~ the product of NDVI and the ~~total~~ near-infrared ~~scene~~ reflectance (NIR). ~~NIRv~~ from moderate
97 spectral resolution satellite imagery and field spectrometers has been shown to empirically track both measured and
98 modelled GPP globally, although ~~with~~ highest uncertainties in the tropics. The NIRv~GPP relationship holds at
99 monthly to seasonal timescales ~~presumably because due to co-incident~~ changes in canopy phenology, ~~influence~~ light
100 capture and ~~scattering, and these changes coincide with changes in~~ GPP (Badgley et al., 2019; Badgley et al., 2017;
101 Dechant et al., 2020). FCVI, derived from radiative transfer theory rather than an empirical relationship, is calculated
102 from RS data by subtracting the reflectance in the NIR from the reflectance in the visible range (Yang et al., 2020).
103 Yang et al. (2020) demonstrated that FCVI tracked GPP and solar-induced fluorescence (SIF; a radiance-based
104 indicator of GPP), by capturing structure and radiation information from a vegetated canopy; ~~tracked GPP~~ in field
105 experiments with crops and in numerical experiments. Yet FCVI showed differences from NIRv due to exposed soil
106 within the vegetated study areas. In previous studies, FCVI and NIRv were similar for dense green canopies where
107 soils have less of an impact, but this has not yet been tested in the tropics (Wang et al., 2020; Badgley et al., 2019;
108 Dechant et al., 2020). ~~The product of NDVI and the NIR radiance, called NIRvrad,~~ was proposed as a proxy for GPP
109 on half-hourly and daily timescales. ~~In contrast, to~~ NIRv and FCVI ~~which~~ track changes on longer timescales (Wu
110 et al., 2020; Dechant et al., 2020; Baldocchi et al., 2020; Zeng et al., 2019). ~~NIRvrad is calculated by multiplying
111 NDVI by the NIR radiance~~ Because the radiance of NIR accounts for incoming radiation at short timescales, NIRvrad
112 has tracked GPP and SIF on half-hourly and diurnal scales as well as seasonally in crops and, to a limited extent,
113 natural grass and savanna ecosystems (Dechant et al., 2020; Baldocchi et al., 2020; Zeng et al., 2019; Wu et al., 2020).

114 Readily available UAS-based hyperspectral sensors are capable of robust measurements of NIRv, FCVI, and
115 NIRvrad at ultra-high spatial scales, i.e. ~~in~~ tens of centimeters **or less**. In this regard, UAS-based data have the potential
116 to improve our understanding of tropical forest structure and function over a range of scales that are poorly resolved
117 by other RS platforms. Here, we use high spatial resolution UAS measurements to characterize spatial and temporal
118 variation in a semi-deciduous tropical forest canopy during the dry season, and compare commonly used spectral
119 indices (NDVI and EVI) to newer vegetation indicators (NIRv, NIRvrad, and FCVI) by (i) examining correlations
120 between GPP and vegetation indicators using mean values across the canopy throughout the day, (ii) evaluating the
121 distribution of fine spatial resolution values (~15 cm) across the canopy and examining changes in this spatial variation
122 throughout the course of two days, and finally (iii) identifying the dominant spatial scale driving variation across our
123 10 ha study region.

124 **2 Materials and Methods**

125 **2.1 Study Area**

126 Barro Colorado Island (BCI), Panama, is a 1560 ha island (approximately 15 km²) in Gatun Lake, which was formed
127 by the construction of the Panama Canal. The Smithsonian Tropical Research Institute manages the preserved area
128 specifically for research. This semi-deciduous moist tropical forest receives approximately 2640 mm mean annual
129 precipitation and has a mean temperature of 26°C with a dry season from approximately January through April (Detto
130 et al., 2018). There is high species diversity, with approximately 500 tree species, approximately 60 species per ha,
131 and about 6.3% of trees at >30cm diameter at breast height (dbh) (Bohlmann and O'Brien, 2006; Condit et al., 2000).
132 The UAS and ground measurements were focused on an area approximately 10 ha within the footprint of an eddy
133 covariance tower near the center of the island (9.156440°, -79.848210°).

134 **2.2 Data collection**

135 The GatorEye Unmanned Flying Laboratory is a hardware and software system built for sensor fusion
136 applications, and which includes hyperspectral, thermal, and visual cameras and a Lidar sensor, coupled with a
137 differential GNSS, internal hard drives, computing systems, and an Inertial Motion Unit (IMU). Hardware and
138 processing details, as well as data downloads, are available at www.gatoreye.org. The GatorEye flew 13 missions on
139 January 30 and 31, 2019 over the forest canopy within the eddy covariance tower footprint at an average height of 120
140 m above ground level (AGL) and at 12 m/s (Fig. 1). In this study, we used radiometrically calibrated flight transects
141 from the Nano VNIR 270 spectral band hyperspectral sensor (Headwall Photonics, Fitchburg, MA, USA) which
142 covered approximately 1 ha per flight within the EC footprint in this study. The Nano **sensor** spectrally samples at
143 approximately 2.2 nm and 12-bit radiometric resolution from 400 to 1050 nm. The frame rate was set to 100 fps, with
144 an integration time of 12 ms and provided a pixel resolution of approximately 15x15 cm. The Nano was calibrated to
145 radiance by the manufacturer before the field campaign and pixel drift was removed by dark images collection, which
146 was corrected for during the conversion from digital number to radiance. The hyperspectral transects were equally
147 subset for each flight in ENVI + IDL (Harris Geospatial, Boulder, CO). Each flight resulted in 1920 transects of

148 approximately 400 m length composing three blocks discretized in 2500 data points. Simultaneous lidar was collected
149 using a VLP-32c ultra puck (Velodyne, San Jose, CA), which was processed to a 0.5x0.5 m resolution digital surface
150 model (DSM).

151 Turbulent fluxes and meteorological variables were measured from a 40 m Eddy Covariance (EC) flux tower
152 (Fig. 1). The eddy covariance system includes a sonic anemometer (CSAT3, Campbell Scientific, Logan, UT) and an
153 open-path infrared CO₂/H₂O gas analyzer (LI7500, LiCOR, Lincoln, NE). High-frequency (10Hz) measurements
154 were acquired by a datalogger (CR1000, Campbell Scientific) and stored on a local PC. Other measurements made at
155 the tower include air temperature and relative humidity (HC2S3, Rotronic, Hauppauge New York), and
156 photosynthetically active radiation (PAR; BF5, Delta-T Devices, UK). EC data were processed with a custom program
157 using a standard routine described in Detto et al. (2010). GPP was derived from daytime values of net ecosystem
158 exchange (NEE) by adding the corresponding mean daily ecosystem respiration obtained as the intercept of the light
159 response curve (Lasslop et al., 2010). Due to a power issue, EC data ~~corresponding to the~~ were not available ~~onduring~~
160 ~~the~~ January 30 flights ~~was not collected~~; so only January 30 GPP were available.

161 An HH2 Pro Spectroradiometer (HH2; ASD/Panalytical/Malvern, Boulder, CO) fitted with a diffuse cosine
162 receptor was used on the ground in full sun at the forest edge to record incoming irradiance on January 30 and 31,
163 2019 (~ 3nm FWHM and spectral sampling at 1nm). HH2 irradiance was resampled to match the Nano hyperspectral
164 sensor and used to calculate reflectance. A calibrated reference tarp was placed in full sun at the forest edge and the
165 UAS flew over and recorded the tarp each UAS flight. Reflectance was calculated separately using the HH2 and tarp
166 data and resulting reflectance values compared as a method to vicariously cross-calibrate reflectance from the
167 hyperspectral data (<7.0% difference for all data in the study). In addition, PAR was calculated with the HH2 data and
168 compared to the tower-mounted PAR measurement (approximately 1.5 km apart) to help understand any differences
169 in the sky conditions during flight times. PAR differences across the site for each flight time for the duration of flights
170 (approximately 10-15 minutes in length each) ranged between 4.0% and 10.3% .

171

172 2.3 Vegetation indicators

173 We calculated NDVI and EVI as (Tucker, 1979; Huete et al., 2002; Rouse JR et al., 1974):

$$174 \quad NDVI = \frac{R_{770-800} - R_{630-670}}{R_{770-800} + R_{630-670}} \quad (1)$$

and

$$175 \quad EVI = \frac{2.5(R_{770-800} - R_{630-670})}{R_{770-800} + 6 \times R_{630-670} - 6 \times R_{460-475} + 1} \quad (2)$$

176 where R is reflectance and the subscripts indicate wavelengths. Here, we used the averages of 770-800 nm for NIR,
177 630-670 nm for red reflectance, and 460-475 nm for blue bands reflectance and normalized to reduce noise.

178 We further calculated the near-infrared vegetation index NIRv as:

$$179 \quad NIRv = NDVI \times R_{770-800} \quad (3)$$

178 where $R_{770-800}$ is the NIR reflectance (Badgley et al., 2017). The fluorescence correction vegetation index (FCVI)
179 was calculated from spectral data by subtracting the reflectance in the visible range ($R_{400-700}$) from the NIR
180 reflectance (Yang et al., 2020) as follows

$$FCVI = R_{770-800} - R_{400-700} \quad (4).$$

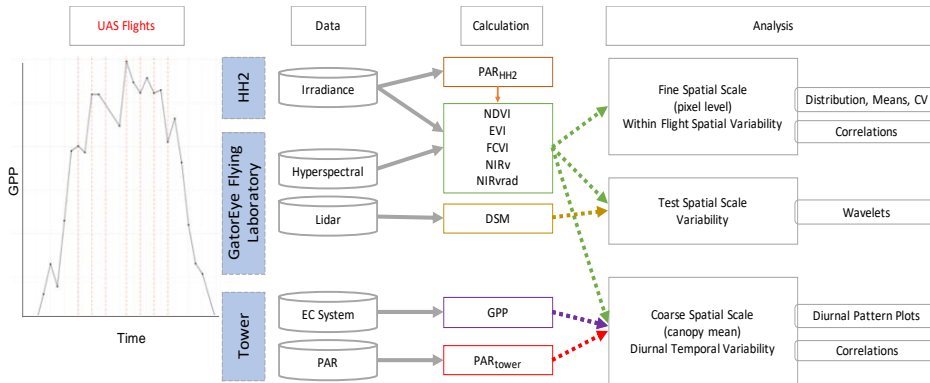
181 The near-infrared radiance of vegetation (NIRvrad) was calculated similarly to the NIRv, except NDVI was multiplied
182 by the radiance, rather than reflectance, from the NIR region ($Rad_{770-800}$) (Wu et al., 2020) as follows:

$$NIRvrad = NDVI \times Rad_{770-800} \quad (5).$$

183 2.4 Data Analysis

184 [A workflow summarizing data analyses is provided in Fig. 1.](#) We examined mean values across the canopy
185 over the course of one day by creating a diurnal time series of scatterplots of the tower-based PAR data, tower-based
186 GPP data, and means of all spectral vegetation indicators, on Jan 31, 2019, and ran comparisons using Pearson's
187 correlation coefficients to examine correlations. [Results are provided in Section 3.1 and Fig. 2.](#) At fine spatial scales,
188 i.e. pixel sizes level-of ~15 cm, we created density plots, calculated the coefficient of variation (CV), and calculated
189 the means of all vegetation indicators (NDVI, EVI, NIRv, FCVI, NIRvrad) for each flight to compare spatial and
190 temporal variability. [Results are provided in Section 3.2 and Fig. 3.](#) To determine which spatial scales dominate the
191 variability of each vegetation quantity, we ran power spectrum wavelet analysis using code created in the Matlab
192 programming language (Mathworks, Natick, Massachusetts). For each vegetation quantity and each flight, and for the
193 lidar elevation model representing canopy height, we computed the Morlet wavelet power spectrum of individual
194 transects (Torrence and Compo, 1998). All power spectra from the wavelet analysis were normalized to unit variance.
195 An ensemble power spectrum for each vegetation indicator was created by averaging across all the transects of each
196 flight and then across flights. We then compared the power spectra for each vegetation indicator and lidar data to
197 compare the spatial scales at which the quantities captured variability as well as the spatial scale at which the lidar-
198 based elevation model captured variability. [Results are provided in Section 3.3 and Fig. 4.](#) For illustration purposes,
199 Fig. S3 is an example of [two synthetic signals generated with fractal Brownian motion algorithm and different level](#)
200 [of noise-to-signal ratio two signals, a higher and lower noise signal created with fractals](#) (Signal A and B, respectively,
201 Fig. A1) and the corresponding power spectra which decay differently at smaller spatial scales (Power Spectra, Fig.
202 A1). Initial UAS data processing was carried out in Interactive Data Language (IDL) and Environment for Visualizing
203 Images (ENVI) (Harris Geospatial, Boulder, CO). Other analyses, including graphical illustrations, were carried out
204 using the R open source environment with libraries dplyr, ggplot, and tidyverse (R Development Core Team, 2010;
205 Wickham et al., 2018; Wickham, 2017, 2016) and Matlab [R2019a](#) (Mathworks, Natick, Massachusetts).

206



207
 208 **Figure 1.** Summary of methods. **Diagram representing discrete flight times for UAS and near-continuous EC-estimated**
 209 **GPP (far left).** Platforms and instrumentation (blue) consisted of the Analytical Spectral Devices (ASD) Handheld
 210 Spectroradiometer Pro 2 (HH2), the GatorEye Flying Laboratory, and the Tower at Barro Colorado Island (BCI). Data
 211 collected included Irradiance, Hyperspectral, Lidar, Eddy Covariance System (EC), and Photosynthetically Active
 212 Radiation (PAR). Calculations made were PAR with the HH2 (PAR_{HH2}), the Normalized Difference Vegetation Index
 213 (NDVI), Enhanced Vegetation Index (EVI), Fluorescence Correction Vegetation Index (FCVI), the Near Infrared
 214 Vegetation Index (NIRv), the Near Infrared Radiance of Vegetation (NIRvrad), the Digital Surface Model (DSM), Gross
 215 Primary Productivity (GPP) and PAR from the PAR Sensor on the Tower (PAR_{tower}). An overview of the data analysis
 216 at each scale is provided in the right of the diagram.

217 **3 Results and discussion**

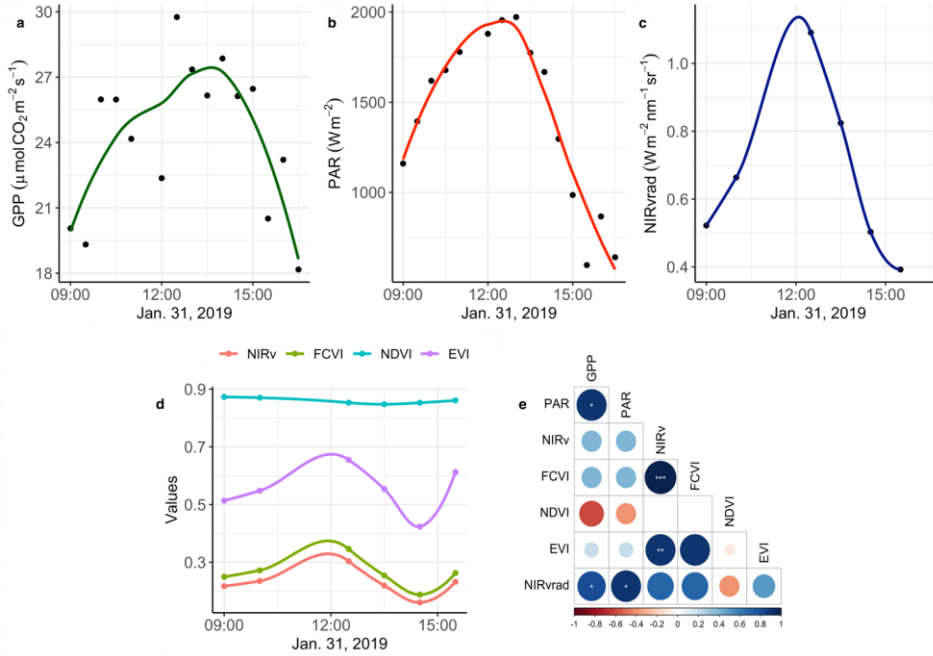
218 **3.1 Diurnal trend in spectral vegetation indicators, PAR, and GPP**

219 The degree to which remote sensing vegetation indicators represent changes in GPP depend largely on canopy
 220 structure-dependent light absorption and scattering processes, that is, ~~exploiting relationships a joint relationship~~
 221 between a remote sensing vegetation quantity, PAR or APAR, and GPP. Fig. 2 shows GPP, PAR, and the mean value
 222 of each vegetation quantity at each flight time over the course of January 31, the day on which we had overlapping
 223 data between the UAS and eddy covariance system (Fig. 2a-d). Additionally, Pearson correlation coefficients among
 224 mean NIRv, FCVI, NIRvrad, EVI, and NDVI for each flight time and the GPP and PAR values at the flight times are
 225 shown in Fig. 2d. NIRv is significantly and strongly positively correlated to both FCVI ($r=0.9$, $p<0.001$) and EVI
 226 ($r=0.9$, $p<0.01$). NIRvrad is the only vegetation quantity with a significant correlation to PAR and GPP, with a strong
 227 positive relationship (0.9 and 0.81, respectively, p -values <0.05 ; Fig. 2d). Mean NIRvrad values also have the greatest
 228 relative diurnal change among the vegetation indicators (Fig. 2c and d). These results demonstrate that a shared
 229 correlation of NIRvrad and GPP to PAR results in mean NIRvrad tracking diurnal changes in GPP to a greater degree
 230 than NIRv, FCVI, NDVI or EVI, because NIRvrad takes incoming radiation into account whereas the other vegetation
 231 indicators do not. ~~The ability of NIRvrad to track APAR is notable alone. However, our This evidence supports the~~
 232 proposed use of NIRvrad as a proxy for changes in GPP on short timescales – ~~albeit based on only one day of data.~~
 233 NIRvrad is ~~also~~ a more ~~practicalefficient measurement-proxy~~ of GPP ~~than SIF~~ in the sense that a separate instrument
 234 to measure PAR is not needed (Wu et al., 2020; Zeng et al., 2019). ~~Given that the relationship between NIRvrad and~~

Commented [SP1]: Reads better if you delete this.

Commented [SP2]: Reads better if you delete this

235 GPP depends on PAR, it is unclear if the association between NIRvrad and GPP would weaken during the wet season
 236 when low light or diffuse light conditions are more common (Berry and Goldsmith, 2020).



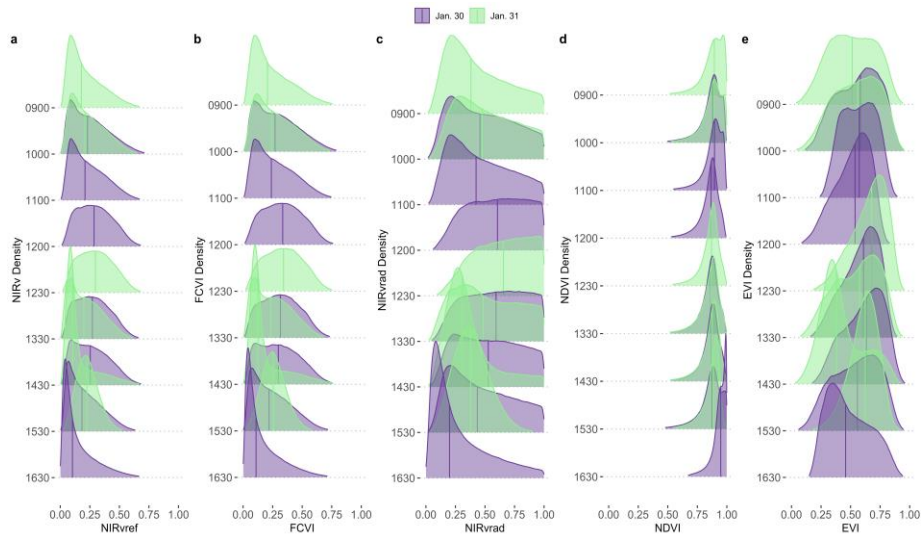
237
 238 **Fig. 2.** Diurnal time series smoothed with a LOESS filter of a) GPP b) PAR c) NIRvrad d) NIRv, FCVI, NDVI, and EVI e)
 239 comparisons of quantities using Pearson correlations color indicates strength of relationship, * = p-value<0.05, ** = p-value
 240 <0.01, *** = p-value <0.001.

241 **3.2 Tropical forest canopy variation**

242 Spatial distributions and the coefficient of variation (CV) of all pixels of NIRv, FCVI, and NIRvrad are
 243 generally similar to one another and show considerable variation spatially across the canopy and temporally over the
 244 course of a day and across days (Fig. 3a-c, Table A2). NIRv, FCVI, and NIRvrad distributions are distinct from EVI
 245 and NDVI (Fig. 3a-e, Table A2, and Table A2). NIRv, FCVI, and NIRvrad have the highest CV at each flight time
 246 (between 39.78% and 91.54%, Table A1), followed by EVI (between 20.24% and 37.24%, Table A2) and NDVI
 247 varied the least at any flight time (between 9.83% and 12.82%, Table A2). For some indices, mean values across the
 248 canopy fail to capture extreme high (NIRv, NIRvrad, and FCVI) or low values (NDVI) during morning and afternoon
 249 hours. This pattern suggests “hot” and “cool” spots of activity related to heterogeneity in forest structure and low sun
 250 angles. In previous studies, the directional effects on NIRv have been examined on coarse spatial scales (i.e. satellites)
 251 and have been proposed as a means of improving understanding of NIRv agreement to GPP (Hao et al., 2021; Dechant
 252 et al., 2020; Baldocchi et al., 2020; Zhang et al., 2020). Our results demonstrate that NIRv, FCVI, and NIRvrad capture
 253 fine-grained heterogeneity of this tropical forest canopy, which was obscured by EVI and NDVI (Fig. 3a-e). NIRv

254 and NIRvrad use NDVI, thus, by definition, NIR is the largest contributing factor to the heterogeneity captured (Fig.
255 3a, c, and e). While NIRv and NIRvrad distributions are generally similar, they diverge in the afternoons when PAR
256 declines, which likely is why NIRvrad is better correlated with GPP. EVI variability was higher than NDVI variability,
257 but lower than that of NIRv, FCVI, and NIRvrad, indicating that EVI has a different level of sensitivity to viewing
258 geometry and canopy components (potentially understory), light absorption and scattering regime of the canopy than
259 the other indices (Table A1 and Table A2). We also show empirically that NIRv and FCVI are virtually the same in a
260 dense tropical forest presumably due to both indices similarly representing the radiation regime of the tropical forest
261 canopy, i.e. light capture and scattering, in conditions with little background soil, supporting the predictions of earlier
262 studies (Dechant et al., 2020; Zeng et al., 2019; Yang et al., 2018b; Wu et al., 2020).

263 Midday distributions of NIRv, FCVI, and NIRvrad on Jan. 30 at 12:00 and 1330 and Jan. 31 at 12:30 are less
264 skewed than at other times of the day whereas morning and afternoon distributions are skewed toward lower values,
265 except for Jan. 31 at 15:30 (Fig. 3a-c). On both days, when mean values peak at midday, the variation for all vegetation
266 indicators is lowest (Jan 30, 1200 CV between 47.6 and 49.2 and Jan 31, 1230 CV between 45.6 and 47.2) (Fig. 3,
267 Table A1). The highest variability occurred in the afternoon on both days (Jan 30, 1630 CV between 91.3% and 91.5
268 and Jan 31, 1430 CV between 83.3% and 83.8% for all quantities) (Fig. 3, Table A2). At midday, NIRv, FCVI, and
269 NIRvrad variability was low and means were high, indicating that viewing and sun geometry drive the higher and
270 lower values during morning and afternoon. This effect is greater in the afternoon than the morning (Fig. 3, Table
271 A2). However, a different pattern is apparent on Jan. 31 during the 1530 flight time when mean values increased from
272 the 1430 flight time means and the CV values were the lowest of any flight observations in the study and this influence
273 appears to be greatest on EVI. It is possible that this was due to another type of effect on illumination geometry, such
274 as wind influencing the UAS, diffuse radiation effects, or hotspot effects.



275
 276 **Fig. 3.** NIRv (a), FCVI (b), and NIRvrad (c) density plots for each flight time on January 30, 2019 (column 1 each panel)
 277 and January 31, 2019 (column 2 each panel). Colours of distributions indicate the flight time and day.

278 **3.3 Power Spectrum Analysis**

279 Power spectrum analysis was used to identify the dominant spatial scales driving variability across the canopy
 280 (Fig. 4). In Fig. 4, the area beneath the curve is proportional to the variance because it is the spectrum divided by the
 281 corresponding scale and then plotted as a function of the log of the scale (example signals and power spectra provided
 282 Fig. A1). Similar to their spatial distributions (Fig. 3), NIRvrad and FCVI are indistinguishable in their dominant
 283 scales of spatial variability (Fig. 3) (Dechant et al., 2020; Zeng et al., 2019). Power spectrum analysis shows a distinct
 284 peak around 50 m spatial scale for NIRv, NIRvrad, FCVI, and EVI, whereas NDVI peaks at approximately 90 m. The
 285 largest tree crown sizes on BCI are on the order of 20–30 m in diameter and the most common crown sizes are between
 286 4–10 m (Fig. A2). Thus, the spatial variability of the vegetation indicators is strongly influenced by larger forest
 287 structures, such as forest gaps and tree clusters, rather than individual tree crowns.

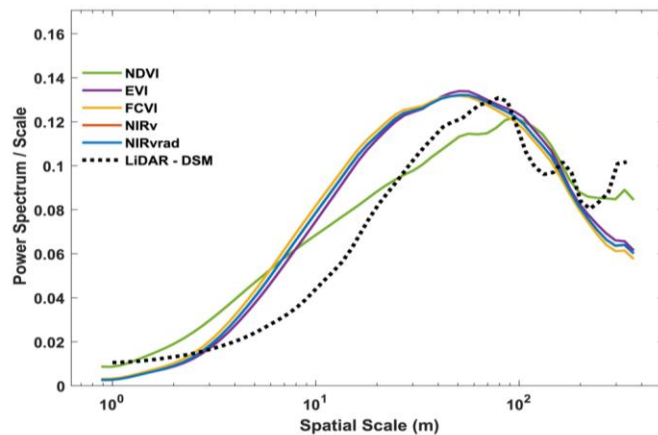
288 This larger scale of variability is also confirmed by the power spectrum of the lidar-derived canopy surface
 289 model, which displays a peak at 70 m scale, indicating that larger than tree crown scales produce the most variability
 290 in canopy height. In other words, UAS-based lidar data also show that canopy heights within a 70 m spatial scale
 291 create strong spatial features on the landscape. Vegetation indicators and the lidar canopy surface model appear less
 292 effective at capturing smaller scale differences within a canopy (leaves or leaf clumps) or among the most frequent
 293 tree crown sizes on BCI (4–10 m sunlit tree crown sizes determined by stereophotos; Fig. A2). However, the peaks
 294 in the vegetation indicators are broader than the peak in the lidar data, showing that smaller features of the canopy are
 295 still contributing to the total spatial signal in the power spectra. These results suggest that satellite data with a spatial
 296 resolution greater than ~50 m may miss important variation in diverse tropical forest canopies. NDVI displays a

297 different shape with a slower decay at small scales, indicating less distinguishable spatial structures from the canopy,
298 and a peak shifted to the larger scales (Fig. 4), i.e. NDVI does not distinguish smaller spatial structures. At much larger
299 scales (>100-200 m), the vegetation indicators decline smoothly, while NDVI and especially lidar show an increase
300 in variance probably associated with topographic heterogeneity.

301 One reason why vegetation indicators and LiDAR captured variability at spatial scales larger than the most
302 common tree crown sizes on BCI is that canopy heights tend to be more uniform on BCI compared to other tropical
303 forests, possibly due to wind (Bohlman and O'Brien, 2006). For example, Dipterocarpus dominated South-East Asian
304 forests have emergent trees, unlike BCI, which can reach up to 60 m in height. Additionally, tree crowns on BCI tend
305 to be more flat-topped than conical or rounded, and trees can be found clumped in similar heights, which could explain
306 why the most often detected unit is larger than the mean of a single crown. On the other end of the spectrum, forest
307 gaps can be larger than a single crown because treefall often affects neighbouring trees.

308 Vegetation indicators and the Lidar-derived surface model represent the spectral and structural properties most
309 broadly of the upper canopy, and thus it is conceivable that they display similar spatial variability. However, NIRv,
310 FCVI, NIRvrad, and EVI discriminated details at a different spatial scale from NDVI and LiDAR. These results
311 parallel the variability detected in their distributions (Fig. 3 and Table A1), where NDVI patterns were distinct from
312 the other vegetation indicators. Taken together, these results show that NIRv, FCVI, and NIRvrad have a smoother
313 spatial pattern and peak at finer scales than NDVI, which is known to saturate at high green biomass (Zhu and Liu,
314 2015; Huete et al., 2002), whereas ~~the emerging vegetation indicators~~ NIRv, FCVI, and NIRvrad should better correlate
315 with aspects of photosynthetic capacity. Thus, these emerging indicators should measure finer resolution spatial
316 heterogeneity and should be more adept at monitoring changes in structure and function of the canopy than NDVI.
317 Additionally, the emerging indicators can potentially disaggregate the physiological and structural component of SIF
318 when SIF measurements are available since changes in structure of the forest coincide with changes in GPP (Wang et
319 al., 2020; Wu et al., 2020; Yang et al., 2020; Dechant et al., 2020). Emerging indicators' heightened ability to
320 differentiate the fine-scale spatial variability in the canopy is likely due to the influence of high upwelling of NIR
321 from the canopy and understory, particularly in the dry season, which tend to blur the signal of the upper canopy for
322 NDVI. Notably, EVI and NDVI, two common indicators of vegetation greenness, show differences in their power
323 spectrum, in particular the slope of the curve for scales less than 20 m. EVI was designed to better capture vegetation
324 changes by exploiting variability in the reflectance in the blue range, especially effective in dense green canopies.
325 This may help explain the scale of variability in this canopy where variation in the blue may be expected to manifest,
326 especially because deciduous crowns, which have high reflectance in blue wavelengths compared to fully leaved
327 crowns, are present on BCI (Bohlman, 2008).

328



329

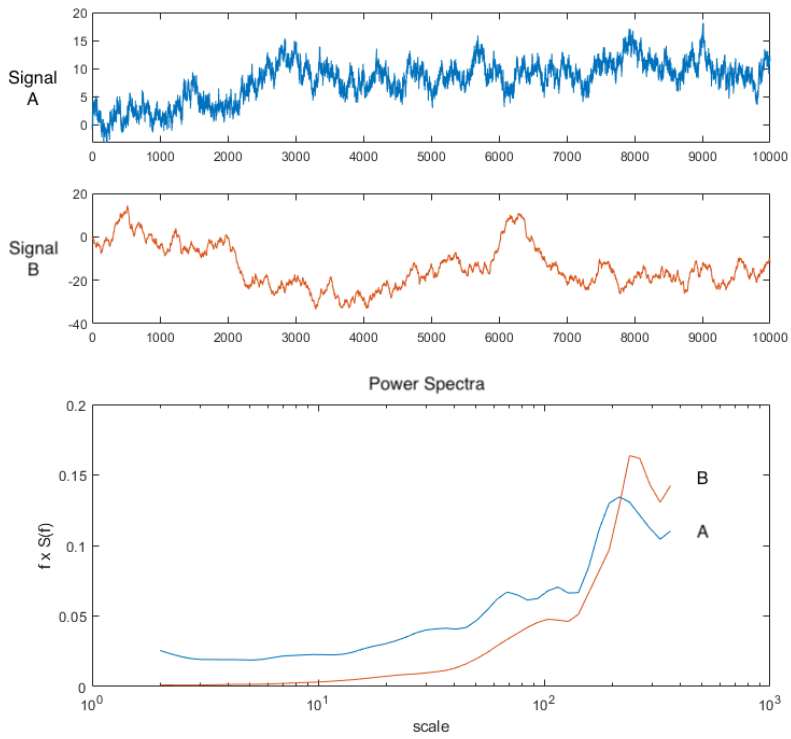
330 **Fig. 4.** Ensemble wavelet power spectra for all the quantities used in this study and a LiDAR-derived digital
 331 surface model (DSM). Note that FCVI and NIRv are similar, thus the NIRv curve is obscured by the FCVI.
 332 Ensembles were created by averaging the spectrum of individual transects, then averaging across flights. Note
 333 that in this representation, the spectrum divided by the corresponding scale as a function of the log of the scale,
 334 the area beneath the curve is proportional to the variance.

335 4 Conclusions

336 We examined NIRv, FCVI, and NIRvrad, emerging vegetation indicators related to fPAR ~~and the scattering of~~
 337 ~~SIF photons,~~ of a semi-deciduous tropical forest canopy using UAS-based hyperspectral data. Our findings
 338 demonstrate that NIRvrad has greater potential to track GPP over the course of a day than the non-radiance-based
 339 ~~indices~~ as evidenced by a shared correlation among NIRvrad, PAR, and GPP. Thus, NIRvrad is a potential proxy for
 340 tracking GPP on short timescales without the need for separate measurements of incoming irradiance. Also, NIRv,
 341 FCVI, and NIRvrad at high spatial resolution (~15cm) unveil greater spatial and diurnal variability of BCI's tropical
 342 forest canopy versus EVI or NDVI, which may pave the way to improve our understanding of the relationship between
 343 GPP and remote sensing observations. ~~For instance, by benchmarking changes of vegetation function and structure~~
 344 ~~that underlie a GPP measurement representing the whole EC footprint, fine scale NIRv, FCVI, or NIRvrad~~
 345 ~~measurements may reveal highly differential behaviors of tropical species diurnally to seasonally.~~ The dominant scale
 346 driving spatial variability of spectral measurements and lidar data are larger forest structures occurring on BCI, such
 347 as groups of similar trees or forest gaps. Yet, smaller, broader peaks in the power spectra of NIRv, FCVI, NIRvrad,
 348 and EVI indicate these four indices incorporate smaller scale information compared to NDVI. Taken together, the
 349 demonstrated potential to track GPP, measure spatial heterogeneity and variability, and capture forest structural
 350 characteristics of BCI open greater possibilities to examine structure and function within and across this tropical forest.

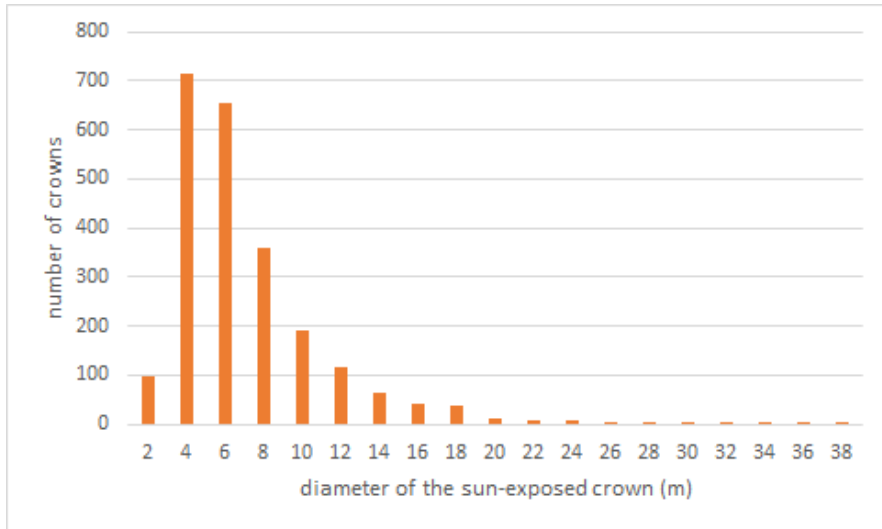
351 Because remote sensing advancements are making it possible to capture physiological responses of vegetation,
 352 the importance of improved techniques to examine the radiation regime, for instance estimating fPAR or APAR, can

353 be overlooked. However, recent studies have highlighted the importance and difficulties of measuring fPAR and
354 APAR, the strong dependence of measurements on illumination and viewing geometry, as well as the need for
355 increased understanding of structure-related radiation regime information more generally e.g. (Hao et al., 2021;
356 Dechant et al., 2020; Baldocchi et al., 2020; Rocha et al., 2021; Zhang et al., 2020). For NIRv, FCVI, and NIRvrad,
357 inclusion of the NIR spectral region makes the emerging indices more sensitive to incoming, absorbed, and scattered
358 radiation, which can be influenced by illumination and viewing geometry, changes in canopy leaf angles or associated
359 structure changes. In the case of NIRvrad, which was most strongly associated with GPP, changes in light regime and
360 associated photosynthetic capacity can even be captured diurnally. Furthermore, NIRv, FCVI, and NIRvrad
361 measurements, especially at high spatial and temporal resolution can help inform our understanding of one another,
362 traditional reflectance-based indices, and other measurements such as SIF. This study highlights the importance of
363 understanding the incoming solar radiation, absorbed and scattered radiation, and illumination and viewing geometry
364 of any remote sensing data, but it also encourages exploiting RS observations to improve our ability to measure
365 structure-related light capture and scattering patterns. It is in this role, we show these measurements should be further
366 investigated as valuable tools to improve our understanding of complex tropical forest canopies and potentially as an
367 improved estimate of fPAR, APAR, or GPP. While this study focuses on BCI, these techniques could be applied more
368 broadly for the purposes of defining the dominant scale of spatial variability, tracking structural changes, monitoring
369 coincident changes in GPP or light regime, or as inputs to vegetation models of tropical forest structure and function.



371
372 **Figure A1.** Sample signals with relatively higher noise (Signal A) and lower noise (Signal B) and their corresponding
373 Power Spectra ensemble plotted as normalized on log scale. Note the representation of the variance by area under the curve
374 is preserved by multiplying the Power ($S(f)$) by the frequency (f). In this way the area beneath the curve is still proportional
375 to the variance.

376



377
 378 **Figure A2.** Distribution of tree crown sizes on BCI in a sample ~10 ha plot taken from digitized high spatial resolution
 379 stereo photos that were linked to stems in the field (Bohlman and Pacala 2012). This ~10 ha plot does not coincide with the
 380 ~10 ha area sampled by the UAS near the eddy covariance tower in this study.

381
 382 **Table A1.** Mean, standard deviation (Sdev) and coefficient of variation (CV) of NIRv, NIRvrad, and FCVI measurements
 383 for the study.

384

Flight Time	Mean	SDev	CV	Mean	SDev	CV	Mean	SDev	CV
	NIRv	NIRv	NIRv (%)	NIRvrad	NIRvrad	NIRvrad (%)	FCVI	FCVI	FCVI (%)
Jan30_1000	0.26	0.16	61.36	0.60	0.36	60.54	0.29	0.18	59.69
Jan30_1100	0.24	0.15	61.48	0.54	0.33	60.56	0.27	0.16	60.89
Jan30_1200	0.29	0.15	49.20	0.82	0.39	47.59	0.34	0.16	47.88
Jan30_1330	0.28	0.14	50.46	0.81	0.40	49.24	0.32	0.16	49.16
Jan30_1430	0.27	0.15	55.46	0.70	0.38	54.38	0.31	0.17	54.22
Jan30_1530	0.21	0.14	65.10	0.63	0.41	64.71	0.25	0.16	64.01
Jan30_1630	0.16	0.14	91.54	0.32	0.30	91.54	0.17	0.15	91.39
Jan31_0900	0.22	0.14	66.31	0.52	0.34	65.25	0.25	0.16	66.01
Jan31_1000	0.24	0.14	59.43	0.66	0.39	58.29	0.27	0.16	59.04
Jan31_1230	0.30	0.14	47.17	1.09	0.50	45.63	0.35	0.16	45.91
Jan31_1330	0.22	0.14	61.91	0.82	0.51	61.47	0.25	0.15	60.53
Jan31_1430	0.16	0.14	85.32	0.50	0.42	83.81	0.19	0.16	83.83

Jan31_1530	0.86	0.08	9.83	0.61	0.12	20.24	0.53	0.04	8.15
------------	------	------	------	------	------	-------	------	------	------

385
386 **Table A2. Mean, standard deviation (Sdev) and coefficient of variation (CV) of NDVI and EVI measurements for the study.**

387

Flight Time	Mean NDVI	SDev NDVI	CV NDVI (%)	Mean EVI	SDev EVI	CV EVI (%)
Jan30_1000	0.86	0.10	11.64	0.57	0.18	31.54
Jan30_1100	0.88	0.09	10.15	0.57	0.14	24.40
Jan30_1200	0.85	0.09	10.38	0.52	0.15	28.48
Jan30_1330	0.85	0.09	10.60	0.59	0.15	25.24
Jan30_1430	0.85	0.09	10.35	0.61	0.16	26.84
Jan30_1530	0.85	0.11	12.52	0.54	0.19	35.21
Jan30_1630	0.93	0.06	6.69	0.49	0.18	36.90
Jan31_0900	0.87	0.10	11.54	0.51	0.19	37.24
Jan31_1000	0.87	0.10	11.08	0.55	0.19	34.66
Jan31_1230	0.85	0.08	9.82	0.66	0.15	22.72
Jan31_1330	0.85	0.09	10.70	0.55	0.19	33.80
Jan31_1430	0.85	0.09	10.58	0.42	0.18	43.07
Jan31_1530	0.86	0.08	9.83	0.61	0.12	20.24

388

389

390

391

392

393 **Code availability**

394 **Data availability**

395 GatorEye data related to this project can be downloaded from www.gatoreye.org. Code and other material
396 with links provided upon request.

397

398 **Author contributions**

399 T.M. designed the study with the help of S.P. and S.A.B.. M.D. and T.M. outfitted the tower and collected tower-
400 based data, T.M. and E.N.B. collected the UAS data. E.N.B., A.M.A.Z., and T.M. pre-processed the hyperspectral and
401 lidar data. T.M. and M.D. further processed UAV, lidar, and GPP data and ran data analysis. M.D., S.P., S.A.B., C.S.,
402 contributed with the methodological framework, data processing analysis and write up T.M., M.D., S.P., S.A.B., C.S.,

403 E.N.B., and A.M.A.Z. contributed to the interpretation, quality control and revisions of the manuscript. All authors
404 read and approved the final version of the manuscript.

405 *Competing interests*

406 The authors declare no conflict of interest.

407 *Acknowledgments*

408 This project execution was carried out while T.M., the primary author, was a Provost's Postdoctoral Fellow
409 in the Department of Geography at Florida State University under the advisement of S.P.. T.M. wishes to extend the
410 sincerest thanks to S.P. for support and guidance, as well as to the FSU Department of Geography, FSU Provost's
411 Postdoctoral Fellows program, and to co-authors who served as mentors. Support for this project, including portions
412 of field logistic and data collection costs and materials, and support for T.M., was provided by the Provost's
413 Postdoctoral Fellows Program at Florida State University. E.N.B. was supported through the School of Forest,
414 Fisheries and Geomatics Sciences and expenses and data collection paid for by T.M.'s Provost's Postdoctoral Fellows
415 Program at Florida State University, A.M.A.Z through the Center for Latin American Studies, and hardware, software,
416 and system costs associated with the GatorEye and data collection were provided through the McIntire Stennis
417 Program of the USDA and the School of Forest, Fisheries and Geomatics Sciences. M.D. was supported by the Carbon
418 Mitigation Initiative at Princeton University. The authors wish to thank the vast support of the collaborators, staff, and
419 researchers at the Smithsonian Tropical Research Institute and, specifically at Barro Colorado Island, without which
420 this research would not be possible. Among other contributors to the work, we also extend special thanks to Alfonso
421 Zambrano, Carli Merrick, Riley Fortier, and Pete Kerby-Miller for field work assistance, and Dr. S. Joseph Wright
422 and Dr. Helene Muller-Landau for support on site as well.

423

424 **References**

425 Alonso, L., Moreno, J., Moya, I., and R. Miller, J. R.: A Comparison of Different Techniques for Passive Measurement
426 of Vegetation Photosynthetic Activity: Solar-Induced Fluorescence, Red-Edge Reflectance Structure and
427 Photochemical Reflectance Indices, *IEEE*, 3, 2003.
428 Alonso, L., Gómez-Chova, L., Vila-Francés, J., Amorós-López, J., Guanter, L., Calpe, J., and Moreno, J.: Sensitivity
429 analysis of the Fraunhofer Line Discrimination method for the measurement of chlorophyll fluorescence using a field
430 spectroradiometer, *IEEE*, 4, 2007.
431 Alonso, L., Gómez-Chova, L., Vila-Francés, J., Amorós-López, J., Guanter, L., Calpe, J., and Moreno, J.: Improved
432 Fraunhofer Line Discrimination Method for Vegetation Fluorescence Quantification, *IEEE GEOSCIENCE AND*
433 *REMOTE SENSING LETTERS*, 5, 5, 2008.
434 Badgley, G., Field, C. B., and Berry, J. A.: Canopy near-infrared reflectance and terrestrial photosynthesis, *Sci Adv*,
435 3, e1602244, 10.1126/sciadv.1602244, 2017.
436 Badgley, G., Anderegg, L. D. L., Berry, J. A., and Field, C. B.: Terrestrial gross primary production: Using NIRV to
437 scale from site to globe, *Glob Chang Biol*, 25, 3731-3740, 10.1111/gcb.14729, 2019.
438 Baldocchi, D. D., Ryu, Y., Dechant, B., Eichelmann, E., Hemes, K., Ma, S., Rey Sanchez, C., Shortt, R., Szutu, D.,
439 Valach, A., Verfaillie, J., Badgley, G., Zeng, Y., and Berry, J. A.: Outgoing Near Infrared Radiation from Vegetation
440 Scales with Canopy Photosynthesis Across a Spectrum of Function, Structure, Physiological Capacity and Weather,
441 *Journal of Geophysical Research: Biogeosciences*, 10.1029/2019jg005534, 2020.

442 [Berry, Z. C., & Goldsmith, G. R.: Diffuse light and wetting differentially affect tropical tree leaf photosynthesis. *New*](#)
443 [Phytologist](#), 225(1), 143-153, 10.1111/nph.16121,2020.

444 [Bohlman, Stephanie. "Hyperspectral remote sensing of exposed wood and deciduous trees in seasonal tropical forests."](#)
445 [In *Hyperspectral remote sensing of tropical and subtropical forests*, pp. 177-192. CRC Press, 2008. Kalacska, M., &](#)
446 [Sanchez-Azofeifa, G. A. \(Eds.\)](#)

447 Bohlman, S. and O'Brien, S.: Allometry, adult stature and regeneration requirement of 65 tree species on Barro
448 Colorado Island, Panama, *Journal of Tropical Ecology*, 22, 123-136, 10.1017/s0266467405003019, 2006.

449 Bohlman, S. and Pacala, S.: A forest structure model that determines crown layers and partitions growth and mortality
450 rates for landscape-scale applications of tropical forests, *Journal of Ecology*, 100, 508-518, 10.1111/j.1365-
451 2745.2011.01935.x, 2012.

452 Castro, A. O., Chen, J., Zang, C. S., Shekhar, A., Jimenez, J. C., Bhattacharjee, S., Kindu, M., Morales, V. H., and
453 Rammig, A.: OCO-2 Solar-Induced Chlorophyll Fluorescence Variability across Ecoregions of the Amazon Basin
454 and the Extreme Drought Effects of El Niño (2015–2016), *Remote Sensing*, 12, 10.3390/rs12071202, 2020.

455 Clark, D. B., Olivas, P. C., Oberbauer, S. F., Clark, D. A., and Ryan, M. G.: First direct landscape-scale measurement
456 of tropical rain forest Leaf Area Index, a key driver of global primary productivity, *Ecol Lett*, 11, 163-172,
457 10.1111/j.1461-0248.2007.01134.x, 2008.

458 Clark, D. A., Asao, S., Fisher, R., Reed, S., Reich, P. B., Ryan, M. G., Wood, T. E., and Yang, X.: Reviews and
459 syntheses: Field data to benchmark the carbon cycle models for tropical forests, *Biogeosciences*, 14, 4663-4690,
460 10.5194/bg-14-4663-2017, 2017.

461 Cogliati, S., Verhoef, W., Kraft, S., Sabater, N., Alonso, L., Vicent, J., Moreno, J., Drusch, M., and Colombo, R.:
462 Retrieval of sun-induced fluorescence using advanced spectral fitting methods, *Remote Sensing of Environment*, 169,
463 344-357, 10.1016/j.rse.2015.08.022, 2015.

464 Condit, R. S., Watts, K., Bohlman, S., Perez, R., Foster, R. B., and Hubbell, S. P.: Quantifying the deciduousness of
465 tropical forest canopies under varying climates, *Journal of Vegetation Science*, 11, 10, 2000.

466 Dechant, B., Ryu, Y., Badgley, G., Zeng, Y., Berry, J. A., Zhang, Y., Goulas, Y., Li, Z., Zhang, Q., Kang, M., Li, J.,
467 and Moya, I.: Canopy structure explains the relationship between photosynthesis and sun-induced chlorophyll
468 fluorescence in crops, *Remote Sensing of Environment*, 241, 10.1016/j.rse.2020.111733, 2020.

469 Detto, M., Baldocchi, D., and Katul, G. G.: Scaling Properties of Biologically Active Scalar Concentration
470 Fluctuations in the Atmospheric Surface Layer over a Managed Peatland, *Boundary-Layer Meteorology*, 136, 407-
471 430, 10.1007/s10546-010-9514-z, 2010.

472 Detto, M., Wright, S. J., Calderon, O., and Muller-Landau, H. C.: Resource acquisition and reproductive strategies of
473 tropical forest in response to the El Niño-Southern Oscillation, *Nature communications*, 9, 913, 10.1038/s41467-018-
474 03306-9, 2018.

475 Frankenberg, C., Fisher, J. B., Worden, J. R., Badgley, G., Saatchi, S. S., Lee, J. E., Toon, G. C., Butz, A., Jung, M.,
476 Kuze, A., and Yokota, T.: New global observations of the terrestrial carbon cycle from GOSAT: Patterns of plant
477 fluorescence with gross primary productivity, *Geophysical Research Letters*, 38, 10.1029/2011gl048738, 2011.

478 Gamon, J. A., Kovalchuck, O., Wong, C. Y. S., Harris, A., and Garrity, S. R.: Monitoring seasonal and diurnal changes
479 in photosynthetic pigments with automated PRI and NDVI sensors, *Biogeosciences*, 12, 4149-4159, 10.5194/bg-12-
480 4149-2015, 2015.

481 Gao, W., Kim, Y., Ustin, S. L., Huete, A. R., Jiang, Z., and Miura, T.: Multisensor reflectance and vegetation index
482 comparisons of Amazon tropical forest phenology with hyperspectral Hyperion data, *Remote Sensing and Modeling*
483 [of Ecosystems for Sustainability IV](#), 10.1117/12.734974, 2007.

484 Gelybó, G., Barcza, Z., Kern, A., and Kljun, N.: Effect of spatial heterogeneity on the validation of remote sensing
485 based GPP estimations, *Agricultural and Forest Meteorology*, 174-175, 43-53, 10.1016/j.agrformet.2013.02.003,
486 2013.

487 Glenn, E. P., Huete, A. R., Nagler, P. L., and Nelson, S. G.: Relationship Between Remotely-sensed Vegetation
488 Indices, Canopy Attributes and Plant Physiological Processes: What Vegetation Indices Can and Cannot Tell Us About
489 the Landscape, *Sensors*, 8, 24, 2008.

490 Guan, K., Pan, M., Li, H., Wolf, A., Wu, J., Medvigy, D., Caylor, K. K., Sheffield, J., Wood, E. F., Malhi, Y., Liang,
491 M., Kimball, J. S., Saleska, Scott R., Berry, J., Joiner, J., and Lyapunin, A. I.: Photosynthetic seasonality of global
492 tropical forests constrained by hydroclimate, *Nature Geoscience*, 8, 284-289, 10.1038/ngeo2382, 2015.

493 Guanter, L., Frankenberg, C., Dudhia, A., Lewis, P. E., Gómez-Dans, J., Kuze, A., Suto, H., and Grainger, R. G.:
494 Retrieval and global assessment of terrestrial chlorophyll fluorescence from GOSAT space measurements, *Remote*
495 [Sensing of Environment](#), 121, 236-251, 10.1016/j.rse.2012.02.006, 2012.

496 Guanter, L., Zhang, Y., Jung, M., Joiner, J., Voigt, M., Berry, J. A., Frankenberg, C., Huete, A. R., Zarco-Tejada, P.,
497 Lee, J. E., Moran, M. S., Ponce-Campos, G., Beer, C., Camps-Valls, G., Buchmann, N., Gianelle, D., Klumpp, K.,

498 Cescatti, A., Baker, J. M., and Griffis, T. J.: Global and time-resolved monitoring of crop photosynthesis with
499 chlorophyll fluorescence, *Proceedings of the National Academy of Sciences of the United States of America*, 111,
500 E1327-1333, 10.1073/pnas.1320008111, 2014.

501 Hao, D., Asrar, G. R., Zeng, Y., Yang, X., Li, X., Xiao, J., Guan, K., Wen, J., Xiao, Q., Berry, J. A., and Chen, M.:
502 Potential of hotspot solar-induced chlorophyll fluorescence for better tracking terrestrial photosynthesis, *Glob Chang*
503 *Biol*, 10.1111/gcb.15554, 2021.

504 Heinsch, F. A., Maosheng, Z., Running, S. W., Kimball, J. S., Nemani, R. R., Davis, K. J., Bolstad, P. V., Cook, B.
505 D., Desai, A. R., Ricciuto, D. M., Law, B. E., Oechel, W. C., Hyojung, K., Hongyan, L., Wofsy, S. C., Dunn, A. L.,
506 Munger, J. W., Baldocchi, D. D., Liukang, X., Hollinger, D. Y., Richardson, A. D., Stoy, P. C., Siqueira, M. B. S.,
507 Monson, R. K., Burns, S. P., and Flanagan, L. B.: Evaluation of remote sensing based terrestrial productivity from
508 MODIS using regional tower eddy flux network observations, *IEEE Transactions on Geoscience and Remote Sensing*,
509 44, 1908-1925, 10.1109/tgrs.2005.853936, 2006.

510 Huete, A., Didan, K., Miura, T., Rodriguez, E. P., Gao, X., and Ferreira, L. G.: Overview of the radiometric and
511 biophysical performance of the MODIS vegetation indices, *Remote Sensing of Environment*, 83, 19, 2002.

512 Huete, A. R., Restrepo-Coupe, N., Ratana, P., Didan, K., Saleska, S. R., Ichii, K., Panuthai, S., and Gamo, M.: Multiple
513 site tower flux and remote sensing comparisons of tropical forest dynamics in Monsoon Asia, *Agricultural and Forest*
514 *Meteorology*, 148, 748-760, 10.1016/j.agrformet.2008.01.012, 2008.

515 Jiang, Z., Huete, A., Didan, K., and Miura, T.: Development of a two-band enhanced vegetation index without a blue
516 band, *Remote Sensing of Environment*, 112, 3833-3845, 10.1016/j.rse.2008.06.006, 2008.

517 Joiner, J., Yoshida, Y., Vasilkov, A. P., Yoshida, Y., Corp, L. A., and Middleton, E. M.: First observations of global
518 and seasonal terrestrial chlorophyll fluorescence from space, *Biogeosciences*, 8, 637-651, 10.5194/bg-8-637-2011,
519 2011.

520 Julitta, T.: Optical proximal sensing for vegetation monitoring, PhD Dissertation, Department of Earth and
521 Environmental Sciences, University of Milano-Bicocca, 136 pp., 2015.

522 Jung, M., Reichstein, M., Margolis, H. A., Cescatti, A., Richardson, A. D., Arain, M. A., Arneth, A., Bernhofer, C.,
523 Bonal, D., Chen, J., Gianelle, D., Gobron, N., Kiely, G., Kutsch, W., Lasslop, G., Law, B. E., Lindroth, A., Merbold,
524 L., Montagnani, L., Moors, E. J., Papale, D., Sottocornola, M., Vaccari, F., and Williams, C.: Global patterns of land-
525 atmosphere fluxes of carbon dioxide, latent heat, and sensible heat derived from eddy covariance, satellite, and
526 meteorological observations, *Journal of Geophysical Research*, 116, 10.1029/2010jg001566, 2011.

527 Köhler, P., Guanter, L., Kobayashi, H., Walther, S., and Yang, W.: Assessing the potential of sun-induced fluorescence
528 and the canopy scattering coefficient to track large-scale vegetation dynamics in Amazon forests, *Remote Sensing of*
529 *Environment*, 769-785, 10.1016/j.rse.2017.09.025, 2017.

530 Lasslop, G., Reichstein, M., Detto, M., Richardson, A. D., and Baldocchi, D. D.: Comment on Vickers et al.: Self-
531 correlation between assimilation and respiration resulting from flux partitioning of eddy-covariance CO₂ fluxes,
532 *Agricultural and Forest Meteorology*, 150, 312-314, 10.1016/j.agrformet.2009.11.003, 2010.

533 Laurance, W. F., Useche, D. C., Rendeiro, J., Kalka, M., Bradshaw, C. J., Sloan, S. P., Laurance, S. G., Campbell, M.,
534 Abernethy, K., Alvarez, P., Arroyo-Rodriguez, V., Ashton, P., Benitez-Malvido, J., Blom, A., Bobo, K. S., Cannon,
535 C. H., Cao, M., Carroll, R., Chapman, C., Coates, R., Cords, M., Danielsen, F., De Dijn, B., Dinerstein, E., Donnelly,
536 M. A., Edwards, D., Edwards, F., Farwig, N., Fashing, P., Forget, P. M., Foster, M., Gale, G., Harris, D., Harrison,
537 R., Hart, J., Karpanty, S., Kress, W. J., Krishnaswamy, J., Logsdon, W., Lovett, J., Magnusson, W., Maisels, F.,
538 Marshall, A. R., McClearn, D., Mudappa, D., Nielsen, M. R., Pearson, R., Pitman, N., van der Ploeg, J., Plumptre, A.,
539 Poulsen, J., Quesada, M., Rainey, H., Robinson, D., Roetgers, C., Rovero, F., Scatena, F., Schulze, C., Sheil, D.,
540 Struhsaker, T., Terborgh, J., Thomas, D., Timm, R., Urbina-Cardona, J. N., Vasudevan, K., Wright, S. J., Arias, G. J.,
541 Arroyo, L., Ashton, M., Auzel, P., Babaasa, D., Babweteera, F., Baker, P., Banki, O., Bass, M., Bila-Isia, I., Blake,
542 S., Brockelman, W., Brokaw, N., Bruhl, C. A., Bunyavejchewin, S., Chao, J. T., Chave, J., Chellam, R., Clark, C. J.,
543 Clavijo, J., Congdon, R., Corlett, R., Dattaraja, H. S., Dave, C., Davies, G., Beisiegel Bde, M., da Silva Rde, N., Di
544 Fiore, A., Diesmos, A., Dirzo, R., Doran-Sheehy, D., Eaton, M., Emmons, L., Estrada, A., Ewango, C., Fedigan, L.,
545 Feer, F., Fruth, B., Willis, J. G., Goodale, U., Goodman, S., Guix, J. C., Guthiga, P., Haber, W., Hamer, K., Herbing,
546 I., Hill, J., Huang, Z., Sun, I. F., Ickes, K., Itoh, A., Ivanauskas, N., Jackes, B., Janovec, J., Janzen, D., Jiangming, M.,
547 Jin, C., Jones, T., Justiniano, H., Kalko, E., Kasangaki, A., Killeen, T., King, H. B., Klop, E., Knott, C., Kone, I.,
548 Kudavidanage, E., Ribeiro, J. L., Lattke, J., Laval, R., Lawton, R., Leal, M., Leighton, M., Lentino, M., Leonel, C.,
549 Lindsell, J., Ling-Ling, L., Linsenmair, K. E., Losos, E., Lugo, A., Lwanga, J., Mack, A. L., Martins, M., McGraw,
550 W. S., McNab, R., Montag, L., Thompson, J. M., Nabe-Nielsen, J., Nakagawa, M., Nepal, S., Norconk, M., Novotny,
551 V., O'Donnell, S., Opiang, M., Ouboter, P., Parker, K., Parthasarathy, N., Pisciotta, K., Prawiradilaga, D., Pringle, C.,
552 Rajathurai, S., Reichard, U., Reinartz, G., Renton, K., Reynolds, G., Reynolds, V., Riley, E., Rodel, M. O., Rothman,
553 J., Round, P., Sakai, S., Sanaïotti, T., Savini, T., Schaab, G., Seidensticker, J., Siaka, A., Silman, M. R., Smith, T. B.,

554 de Almeida, S. S., Sodhi, N., Stanford, C., Stewart, K., Stokes, E., Stoner, K. E., Sukumar, R., Surbeck, M., Tobler,
555 M., Tscharnkte, T., Turkalo, A., Umapathy, G., van Weerd, M., Rivera, J. V., Venkataraman, M., Venn, L., Vereza,
556 C., de Castilho, C. V., Waltert, M., Wang, B., Watts, D., Weber, W., West, P., Whitacre, D., Whitney, K., Wilkie, D.,
557 Williams, S., Wright, D. D., Wright, P., Xiankai, L., Yonzon, P., and Zamzani, F.: Averting biodiversity collapse in
558 tropical forest protected areas, *Nature*, 489, 290-294, 10.1038/nature11318, 2012.

559 Lee, J. E., Frankenberg, C., van der Tol, C., Berry, J. A., Guanter, L., Boyce, C. K., Fisher, J. B., Morrow, E., Worden,
560 J. R., Asefi, S., Badgley, G., and Saatchi, S.: Forest productivity and water stress in Amazonia: observations from
561 GOSAT chlorophyll fluorescence, *Proceedings. Biological sciences / The Royal Society*, 280, 20130171,
562 10.1098/rspb.2013.0171, 2013.

563 Lewis, S. L., Lloyd, J., Sitch, S., Mitchard, E. T. A., and Laurance, W. F.: Changing Ecology of Tropical Forests:
564 Evidence and Drivers, *Annual Review of Ecology, Evolution, and Systematics*, 40, 529-549,
565 10.1146/annurev.ecolsys.39.110707.173345, 2009.

566 Liangyun Liu, X. L., ZhihuiWang, and Bing Zhang: Measurement and Analysis of BidirectionalSIF Emissions in
567 Wheat Canopies, *IEEE TRANSACTIONS ON GEOSCIENCE AND REMOTE SENSING*, 12, 2016.

568 Liu, J., Bowman, K. W., Schimel, D. S., Parazoo, N. C., Jiang, Z., Lee, M., Bloom, A. A., Wunch, D., Frankenberg,
569 C., Sun, Y., O'Dell, C. W., Gurney, K. R., Menemenlis, D., Gierach, M., Crisp, D., and Eldering, A.: Contrasting
570 carbon cycle responses of the tropical continents to the 2015-2016 El Nino, *Science*, 358, eaam5690,
571 10.1126/science.aam5690, 2017.

572 Liu, L., Yang, X., Gong, F., Su, Y., Huang, G., and Chen, X.: The Novel Microwave Temperature Vegetation Drought
573 Index (MTVDDI) Captures Canopy Seasonality across Amazonian Tropical Evergreen Forests, *Remote Sensing*, 13,
574 10.3390/rs13030339, 2021.

575 Liu, X., Liu, L., Zhang, S., and Zhou, X.: New Spectral Fitting Method for Full-Spectrum Solar-Induced Chlorophyll
576 Fluorescence Retrieval Based on Principal Components Analysis, *Remote Sensing*, 7, 10626-10645,
577 10.3390/rs70810626, 2015.

578 Logan, B. A., Adams, W. W., and Demmig-Adams, B.: Viewpoint:Avoiding common pitfalls of chlorophyll
579 fluorescence analysis under field conditions, *Functional Plant Biology*, 34, 853, 10.1071/fp07113, 2007.

580 Magney, T. S., Frankenberg, C., Fisher, J. B., Sun, Y., North, G. B., Davis, T. S., Kornfeld, A., and Siebke, K.:
581 Connecting active to passive fluorescence with photosynthesis: a method for evaluating remote sensing measurements
582 of Chl fluorescence, *The New phytologist*, 1594-1608, 10.1111/nph.14662, 2017.

583 Malenovsky, Z., Mishra, K. B., Zemek, F., Rascher, U., and Nedbal, L.: Scientific and technical challenges in remote
584 sensing of plant canopy reflectance and fluorescence, *Journal of experimental botany*, 60, 2987-3004,
585 10.1093/jxb/erp156, 2009.

586 Malhi, Y.: The productivity, metabolism and carbon cycle of tropical forest vegetation, *Journal of Ecology*, 100, 65-
587 75, 10.1111/j.1365-2745.2011.01916.x, 2012.

588 Medlyn, B. E.: Physiological basis of the light use efficiency model, *Tree Physiology*, 18, 167-176,
589 <https://doi.org/10.1093/treephys/18.3.167>, 1998.

590 Meroni, M., Rossini, M., Guanter, L., Alonso, L., Rascher, U., Colombo, R., and Moreno, J.: Remote sensing of solar-
591 induced chlorophyll fluorescence: Review of methods and applications, *Remote Sensing of Environment*, 113, 2037-
592 2051, 10.1016/j.rse.2009.05.003, 2009.

593 Merrick, Pau, Jorge, Bennartz, and Silva: Spatiotemporal Patterns and Phenology of Tropical Vegetation Solar-
594 Induced Chlorophyll Fluorescence across Brazilian Biomes Using Satellite Observations, *Remote Sensing*, 11,
595 10.3390/rs11151746, 2019.

596 Merrick, T., Jorge, M. L. S. P., Silva, T. S. F., Pau, S., Rausch, J., Broadbent, E. N., and Bennartz, R.: Characterization
597 of chlorophyll fluorescence, absorbed photosynthetically active radiation, and reflectance-based vegetation index
598 spectroradiometer measurements, *International Journal of Remote Sensing*, 41, 6755-6782,
599 10.1080/01431161.2020.1750731, 2020.

600 Mitchard, E. T. A.: The tropical forest carbon cycle and climate change, *Nature*, 559, 527-534, 10.1038/s41586-018-
601 0300-2, 2018.

602 Monteith, J.L.: Climate and the efficiency of crop production in Britain, *Phil. Trans. R. Soc. Land.*, 281, 277-294,
603 1977.

604 Morton, D. C., Rubio, J., Cook, B. D., Gastellu-Etchegorry, J. P., Longo, M., Choi, H., Hunter, M. O., and Keller, M.:
605 Amazon forest structure generates diurnal and seasonal variability in light utilization, *Biogeosciences Discussions*,
606 12, 19043-19072, 10.5194/bgd-12-19043-2015, 2015.

607 Morton, D. C., Nagol, J., Carabajal, C. C., Rosette, J., Palace, M., Cook, B. D., Vermote, E. F., Harding, D. J., and
608 North, P. R.: Amazon forests maintain consistent canopy structure and greenness during the dry season, *Nature*, 506,
609 221-224, 10.1038/nature13006, 2014.

610 Moya, I., Camenen, L., Evain, S., Goulas, Y., Cerovic, Z. G., Latouche, G., Flexas, J., and Ounis, A.: A new instrument
611 for passive remote sensing1. Measurements of sunlight-induced chlorophyll fluorescence, *Remote Sensing of*
612 *Environment*, 91, 186-197, 10.1016/j.rse.2004.02.012, 2004.

613 Plascyk, J. A.: The MK II Fraunhofer Line Discriminator (FLD -II) for Airborne and Orbital Remote Sensing of Solar-
614 Stimulated Luminescence, *Optical Engineering*, 14, 8, 1975.

615 Porcar-Castell, A., Tyystjarvi, E., Atherton, J., van der Tol, C., Flexas, J., Pfundel, E. E., Moreno, J., Frankenberg, C.,
616 and Berry, J. A.: Linking chlorophyll a fluorescence to photosynthesis for remote sensing applications: mechanisms
617 and challenges, *Journal of experimental botany*, 65, 4065-4095, 10.1093/jxb/eru191, 2014.

618 R Development Core Team: R: A language and environment for statistical computing, R Foundation for Statistical
619 Computing [code], 2010.

620 Rocha, A. V., Appel, R., Bret-Harte, M. S., Euskirchen, E. S., Salmon, V., and Shaver, G.: Solar position confounds
621 the relationship between ecosystem function and vegetation indices derived from solar and photosynthetically active
622 radiation fluxes, *Agricultural and Forest Meteorology*, 298-299, 10.1016/j.agrformet.2020.108291, 2021.

623 Rong Li, F. Z.: Accuracy assessment on reconstruction algorithms of solar-induced Fluorescence Spectrum,
624 *Geoscience and Remote Sensing Symposium (IGARSS) IEEE International*, 1727-1730,

625 Rossini, M., Alonso, L., Cogliati, S., Damm, A., Guanter, L., Julitta, T., Meroni, M., Moreno, J., Panigada, C., Pinto,
626 F., Rascher, U., Schickling, A., Schüttemeyer, D., Zemek, F., and Colombo, R.: Measuring sun-induced chlorophyll
627 fluorescence: An evaluation and synthesis of existing field data, 5th International workshop on remote sensing of
628 vegetation fluorescence, Paris, France, 1-5,

629 Rouse Jr, J. W., Haas, R. H., Schell, J. A., and Deering, D. W.: Paper A 20, hird Earth Resources Technology Satellite-
630 1 Symposium: The Proceedings of a Symposium Goddard Space Flight Center at Washington, DC 309,

631 Running, S. W., Nemani, R. R., Heinsch, F. A., Zhao, M., Reeves, M., and Hashimoto, H.: A Continuous Satellite-
632 Derived Measure of Global Terrestrial Primary Production, *BioScience*, 54, 547-551, 2004.

633 Ryu, Y., Jiang, C., Kobayashi, H., and Detto, M.: MODIS-derived global land products of shortwave radiation and
634 diffuse and total photosynthetically active radiation at 5 km resolution from 2000, *Remote Sensing of Environment*,
635 204, 812-825, 10.1016/j.rse.2017.09.021, 2018.

636 Saatchi, S. S., Harris, N. L., Brown, S., Lefsky, M., A., E. T., Mitchare, W. S., Zutta, B. R., Buerman, W., Lewis, S.
637 L., Hagen, S., Petrova, S., White, L., Silman, M., and Morel, A.: Benchmark map of forest carbon stocks in tropical
638 regions across three continents, *Proceedings of the National Academy of Sciences*, 108, 9899-9905, 2010.

639 Saatchi, S. S., Harris, N. L., Brown, S., Lefsky, M., Mitchard, E. T., Salas, W., Zutta, B. R., Buermann, W., Lewis, S.
640 L., Hagen, S., Petrova, S., White, L., Silman, M., and Morel, A.: Benchmark map of forest carbon stocks in tropical
641 regions across three continents, *Proceedings of the National Academy of Sciences of the United States of America*,
642 108, 9899-9904, 10.1073/pnas.1019576108, 2011.

643 Samanta, A., Ganguly, S., and Myneni, R.: MODIS Enhanced Vegetation Index data do not show greening of Amazon
644 forests during the 2005 drought, *New Phytologist*, 189, 4, 2010.

645 Schickling, A., Matveeva, M., Damm, A., Schween, J., Wahner, A., Graf, A., Crewell, S., and Rascher, U.: Combining
646 Sun-Induced Chlorophyll Fluorescence and Photochemical Reflectance Index Improves Diurnal Modeling of Gross
647 Primary Productivity, *Remote Sensing*, 8, 574, 10.3390/rs8070574, 2016.

648 Sims, D., Rahman, A., Cordova, V., Elmasri, B., Baldocchi, D., Bolstad, P., Flanagan, L., Goldstein, A., Hollinger,
649 D., and Misson, L.: A new model of gross primary productivity for North American ecosystems based solely on the
650 enhanced vegetation index and land surface temperature from MODIS, *Remote Sensing of Environment*, 112, 1633-
651 1646, 10.1016/j.rse.2007.08.004, 2008.

652 Springer, K., Wang, R., and Gamon, J. A.: Parallel Seasonal Patterns of Photosynthesis, Fluorescence, and Reflectance
653 Indices in Boreal Trees, *Remote Sensing*, 9, 1-18, 10.3390/rs9070691, 2017.

654 Sun, Y., Frankenberg, C., Wood, J. D., Schimel, D. S., Jung, M., Guanter, L., Drewry, D. T., Verma, M., Porcar-
655 Castell, A., Griffiths, T. J., Gu, L., Magney, T. S., Kohler, P., Evans, B., and Yuen, K.: OCO-2 advances photosynthesis
656 observation from space via solar-induced chlorophyll fluorescence, *Science*, 358, eaam5747,
657 10.1126/science.aam5747, 2017.

658 Torrence, C. and Compo, G. P.: A Practical Guide to Wavelet Analysis, *Bulletin of the American Meteorological*
659 *Society*, 79, 61-79, 1998.

660 Tucker, C., Red and photographic infrared linear combinations for vegetation monitoring, *Remote Sensing of*
661 *Environment*, 8, 127-150,1979.

662 Turner, D. P., Ritts, W. D., Cohen, W. B., Gower, S. T., Zhao, M., Running, S. W., Wofsy, S. C., Urbanski, S., Dunn,
663 A. L., and Munger, J. W.: Scaling Gross Primary Production (GPP) over boreal and deciduous forest landscapes in
664 support of MODIS GPP product validation, *Remote Sensing of Environment*, 88, 256-270, 10.1016/j.rse.2003.06.005,
665 2003.

666 Van Wittenberghe, S., Alonso, L., Verrelst, J., Moreno, J., and Samson, R.: Bidirectional sun-induced chlorophyll
667 fluorescence emission is influenced by leaf structure and light scattering properties — A bottom-up approach, *Remote*
668 *Sensing of Environment*, 158, 169-179, 10.1016/j.rse.2014.11.012, 2015.

669 Van Wittenberghe, S., Alonso, L., Verrelst, J., Hermans, I., Delegido, J., Veroustraete, F., Valcke, R., Moreno, J., and
670 Samson, R.: Upward and downward solar-induced chlorophyll fluorescence yield indices of four tree species as
671 indicators of traffic pollution in Valencia, *Environmental pollution*, 173, 29-37, 10.1016/j.envpol.2012.10.003, 2013.

672 Wang, C., Beringer, J., Hutley, L. B., Cleverly, J., Li, J., Liu, Q., and Sun, Y.: Phenology Dynamics of Dryland
673 Ecosystems Along the North Australian Tropical Transect Revealed by Satellite Solar-Induced Chlorophyll
674 Fluorescence, *Geophysical Research Letters*, 46, 5294-5302, 10.1029/2019gl082716, 2019.

675 Wang, S., Zhang, Y., Ju, W., Qiu, B., and Zhang, Z.: Tracking the seasonal and inter-annual variations of global gross
676 primary production during last four decades using satellite near-infrared reflectance data, *The Science of the total*
677 *environment*, 755, 142569, 10.1016/j.scitotenv.2020.142569, 2020.

678 Wickham, H.: *ggplot2: Elegant Graphics for Data Analysis*, Springer-Verlag [code], 2016.

679 Wickham, H.: *tidyverse: Easily Install and Load the 'Tidyverse' (R package*
680 *version 1.2.1) [code]*, 2017.

681 Wickham, H., François, R., Henry, L., and Müller, K.: *dplyr: A Grammar of Data Manipulation (R package version*
682 *0.7.8) [code]*, 2018.

683 Wright, S. J.: The future of tropical forests, *Ann N Y Acad Sci*, 1195, 1-27, 10.1111/j.1749-6632.2010.05455.x, 2010.

684 Wu, G., Guan, K., Jiang, C., Peng, B., Kimm, H., Chen, M., Yang, X., Wang, S., Suyker, A. E., Bernacchi, C. J.,
685 Moore, C. E., Zeng, Y., Berry, J. A., and Cendrero-Mateo, M. P.: Radiance-based NIRv as a proxy for GPP of corn
686 and soybean, *Environmental Research Letters*, 15, 10.1088/1748-9326/ab65cc, 2020.

687 Xu, L., Saatchi, S. S., Yang, Y., Myneni, R. B., Frankenberg, C., Chowdhury, D., and Bi, J.: Satellite observation of
688 tropical forest seasonality: spatial patterns of carbon exchange in Amazonia, *Environmental Research Letters*, 10,
689 084005, 10.1088/1748-9326/10/8/084005, 2015.

690 Yang, H., Yang, X., Zhang, Y., Heskell, M. A., Lu, X., Munger, J. W., Sun, S., and Tang, J.: Chlorophyll fluorescence
691 tracks seasonal variations of photosynthesis from leaf to canopy in a temperate forest, *Glob Chang Biol*, 23,
692 2874-2886, 10.1111/gcb.13590, 2017.

693 Yang, J., Tian, H., Pan, S., Chen, G., Zhang, B., and Dangal, S.: Amazon droughts and forest responses: Largely
694 reduced forest photosynthesis but slightly increased canopy greenness during the extreme drought of 2015/2016, *Glob*
695 *Chang Biol*, 1919-1934, 10.1111/gcb.14056, 2018a.

696 Yang, K., Ryu, Y., Dechant, B., Berry, J. A., Hwang, Y., Jiang, C., Kang, M., Kim, J., Kimm, H., Kornfeld, A., and
697 Yang, X.: Sun-induced chlorophyll fluorescence is more strongly related to absorbed light than to photosynthesis at
698 half-hourly resolution in a rice paddy, *Remote Sensing of Environment*, 216, 658-673, 10.1016/j.rse.2018.07.008,
699 2018b.

700 Yang, P., van der Tol, C., Campbell, P. K. E., and Middleton, E. M.: Fluorescence Correction Vegetation Index
701 (FCVI): A physically based reflectance index to separate physiological and non-physiological information in far-red
702 sun-induced chlorophyll fluorescence, *Remote Sensing of Environment*, 240, 10.1016/j.rse.2020.111676, 2020.

703 Yuan, W., Cai, W., Xia, J., Chen, J., Liu, S., Dong, W., Merbold, L., Law, B., Arain, A., Beringer, J., Bernhofer, C.,
704 Black, A., Blanken, P. D., Cescatti, A., Chen, Y., Francois, L., Gianelle, D., Janssens, I. A., Jung, M., Kato, T., Kiely,
705 G., Liu, D., Marcolla, B., Montagnani, L., Raschi, A., Rouspard, O., Varlagin, A., and Wohlfahrt, G.: Global
706 comparison of light use efficiency models for simulating terrestrial vegetation gross primary production based on the
707 LaThuile database, *Agricultural and Forest Meteorology*, 192-193, 108-120,
708 <https://doi.org/10.1016/j.agrformet.2014.03.007>, 2014.

709 Zarco-Tejada, P. J., González-Dugo, V., and Berni, J. A. J.: Fluorescence, temperature and narrow-band indices
710 acquired from a UAV platform for water stress detection using a micro-hyperspectral imager and a thermal camera,
711 *Remote Sensing of Environment*, 117, 322-337, 10.1016/j.rse.2011.10.007, 2012.

712 Zarco-Tejada, P. J., Morales, A., Testi, L., and Villalobos, F. J.: Spatio-temporal patterns of chlorophyll fluorescence
713 and physiological and structural indices acquired from hyperspectral imagery as compared with carbon fluxes
714 measured with eddy covariance, *Remote Sensing of Environment*, 133, 102-115, 10.1016/j.rse.2013.02.003, 2013.

715 Zarco-Tejada, P. J., Miller, J. R., Mohammed, G. H., Noland, T. L., and Sampson, P. H.: Estimation of chlorophyll
716 fluorescence under natural illumination from hyperspectral data, *International Journal of Applied Earth Observation*
717 *and Geoinformation*, 3, 7, 2001.

718 Zeng, Y., Badgley, G., Dechant, B., Ryu, Y., Chen, M., and Berry, J. A.: A practical approach for estimating the
719 escape ratio of near-infrared solar-induced chlorophyll fluorescence, *Remote Sensing of Environment*, 232,
720 10.1016/j.rse.2019.05.028, 2019.

721 Zhang, Z., Zhang, Y., Zhang, Q., Chen, J. M., Porcar-Castell, A., Guanter, L., Wu, Y., Zhang, X., Wang, H., Ding,
722 D., and Li, Z.: Assessing bi-directional effects on the diurnal cycle of measured solar-induced chlorophyll fluorescence
723 in crop canopies, *Agricultural and Forest Meteorology*, 295, 10.1016/j.agrformet.2020.108147, 2020.
724 Zhang, Z., Zhang, Y., Zhang, Y., Gobron, N., Frankenberg, C., Wang, S., and Li, Z.: The potential of satellite FPAR
725 product for GPP estimation: An indirect evaluation using solar-induced chlorophyll fluorescence, *Remote Sensing of*
726 *Environment*, 240, 10.1016/j.rse.2020.111686, 2020.
727 Zhao, M., Running, S., Heinsch, F. A., and Nemani, R.: MODIS-Derived Terrestrial Primary Production, 11, 635-
728 660, 10.1007/978-1-4419-6749-7_28, 2010.
729 Zhu, X. and Liu, D.: Improving forest aboveground biomass estimation using seasonal Landsat NDVI time-series,
730 *ISPRS Journal of Photogrammetry and Remote Sensing*, 102, 222-231, 10.1016/j.isprsjprs.2014.08.014, 2015.
731
732